AGU PUBLICATIONS

Geochemistry, Geophysics, Geosystems

RESEARCH ARTICLE
10.1002/2016GC006530

Effect of graphite on the electrical conductivity of the lithospheric mantle

Baohua Zhang [1,2] **and Takashi Yoshino** [2]

[1]Key Laboratory for High-Temperature and High-Pressure Study of the Earth's Interior, Institute of Geochemistry, Chinese Academy of Sciences, Guiyang, China, [2]Institute for Planetary Materials, Okayama University, Tottori-ken, Japan

Key Points:
- We report the electrical conductivity of C-bearing and C-coated olivine bicrystal systems
- Graphite film on olivine grain boundary is not stable under upper mantle conditions
- Graphite cannot explain the high-conductivity anomalies in the lithospheric mantle

Correspondence to:
B. Zhang,
zhangbaohua@vip.gyig.ac.cn

Citation:
Zhang, B., and T. Yoshino (2017), Effect of graphite on the electrical conductivity of the lithospheric mantle, *Geochem. Geophys. Geosyst.*, *18*, 23–40, doi:10.1002/2016GC006530.

Received 12 JUL 2016
Accepted 25 NOV 2016
Accepted article online 20 DEC 2016
Published online 10 JAN 2017

Abstract Graphite is considered as one of candidate to explain the high-conductivity anomalies revealed through magnetotelluric (MT) observations. To investigate the effect of interfacial energy on the interconnection of graphite in olivine matrix, we measured the electrical conductivity of polycrystalline San Carlos olivine mixed with 0.8 vol % graphite on the grain boundaries via impedance spectroscopy at 1 GPa and 300–1700 K in a cubic multianvil apparatus. The olivine-graphite dihedral angle of the recovered sample was also measured to determine interfacial energy between graphite and olivine. The bulk electrical conductivities and large activation enthalpy (~1.32 eV) of the carbon-bearing sample were consistent with those of dry polycrystalline olivine. This behavior implies that graphite cannot be interconnected on olivine grain boundaries, which is also supported by the large dihedral angle (98°) of the olivine/graphite system. Impedance spectroscopy measurements were performed at 3 GPa and a temperature of up to 1700 K for carbon-coated olivine bicrystal samples to investigate the stability of graphite films on the grain boundaries of silicate minerals under upper-mantle conditions. The conductivities rapidly or slowly dropped as a function of time and graphite film thickness during annealing at the target temperature. This phenomenon exhibits that graphite film on the olivine grain boundary is readily destroyed under upper-mantle conditions as supported by microstructural observations on the recovered carbon-coated olivine bicrystal samples. Higher interfacial energy and larger dihedral angle (~98°) between graphite and olivine would not allow the maintenance of graphite film on olivine grain boundaries. The activation enthalpy for the apparent disconnection rate of a graphite film on olivine grain boundaries is close to that of carbon diffusion in olivine grain boundaries, which suggests that the disconnection of the graphite film is likely to be controlled by carbon grain boundary diffusion. Therefore, graphite is an unlikely candidate to explain the high-conductivity anomalies revealed by MT surveys in the upper mantle.

1. Introduction

Magnetotelluric (MT) and geomagnetic deep sounding (GDS) occasionally revealed ubiquitous presence of high-conductivity anomaly zone in the upper mantle [e.g., *Shankland and Waff*, 1977; *Jones and Ferguson*, 2001; *Jones et al*., 2003; *Evans et al*., 2005]. These high-conductivity anomalies have been found in both tectonically active regions, such as the East Pacific Rise [*Evans et al*., 2005; *Baba et al*., 2006] and the Middle America trench offshore of Nicaragua [*Naif et al*., 2013], and stable shield areas, such as the cratonic lithosphere [*Jones et al*., 2003, 2009a; *Bologna et al*., 2011], over the depth range of approximately 6–150 km. Representative conductivity values encompass the order of 10^{-2} to $10^{-0.5}$ S/m, which is distinctly higher than the conductivities of surrounding rocks. Thus, the observed high-conductivity anomalies cannot be explained by dominant constituent minerals (especially olivine) without considering the presence of a conductive phase.

During the past several decades, the origin of conductivity anomalies in the lithospheric mantle has given rise to long-standing debates [*Jones*, 1999]. Several potential candidates have been proposed to account for this issue, including aqueous fluids [e.g., *Shankland and Ander*, 1983; *Shimojuku et al*., 2012, 2014], water in nominally anhydrous minerals [*Karato*, 1990; *Wang et al*., 2006; *Karato and Wang*, 2013; *Dai and Karato*, 2014; *Gardés et al*., 2014], graphite [*Jones et al*., 2003; *Pinto et al*., 2010; *Bologna et al*., 2011; *Watson et al*., 2010; *Wang et al*., 2013], partial melting [*Shankland and Waff*, 1977; *Drury*, 1978; *Shankland et al*., 1981; *Yoshino et al*., 2010; *Ni et al*., 2011; *Zhang et al*., 2014; *Chantel et al*., 2016], and other conductive phases, such as sulfides [*Watson et al*., 2010] and magnetite-bearing serpentinite [*Kawano et al*., 2012]. The tectonically stable cratonic lithosphere is generally believed to have depleted water and low-temperature

conditions. Thus, hydrous mantle minerals and partial melting are discarded in such regions. Given that fluids are gravitationally unstable over geological time scales, sulfides are not volumetrically abundant [*Ducea and Park*, 2000]. They are also unstable at depths greater than the uppermost mantle. Consequently, fluids and interconnected sulfides are unlikely to account for the significant conductivity anomalies in the stable cratonic mantle [*Jones et al*., 2003; *Watson et al*., 2010; *Bologna et al*., 2011]. Recent electromagnetic surveys [*Pinto et al*., 2010] revealed a richness of conductivity anomalies on different scales in the lithosphere beneath the Brazilian craton. The anomalies reach conductivity values close to 10^{-1} S/m at 120–140 km depth, where they are at least three orders of magnitude more conductive than the adjacent lithosphere underlying the NW Paraná basin. Similar phenomena were also discovered in the Slave craton in Canada [*Jones et al*., 2003] and in the Gawler craton in Australia [*Selway*, 2014]. These observations have been interpreted to be caused by either graphite or incipient carbonatite melting [*Sifré et al*., 2014, 2015]. On the other hand, *Chen et al*. [2009] reported the spatial overlap between a seismic discontinuity and a conductive anomaly at ~100 km depth in the central Slave craton. This overlap is likely caused by a metasomatized mantle from a Paleoarchean subduction zone and an accretion of lithospheric fragments. Meanwhile, horizontal high-conductivity anomalies observed in the Brazilian craton are probably related to continent-continent collisions and magmatic events [*Bologna et al*., 2011]. Some studies have proposed the presence of either graphite or interconnected films of graphite deposited along grain boundaries as an origin of the high-conductivity anomalies detected in such relatively active areas of the lithospheric mantle [*Chen et al*., 2009; *Bologna et al*., 2011].

Carbon can be present throughout the crust and down to the upper mantle [*Hazen et al*., 2012], and its electrical conductivities are approximately 10^3-10^5 times greater than those of seawater or silicate melt if it exists as graphite. Thus, even a small amount of carbon can significantly increase the electrical conductivity of a rock. Knowledge of the distribution and origin of carbon and carbonaceous phases in the mantle is important in constraining its role in several mantle processes. *Pearson et al*. [1994] have demonstrated that graphite crystals in peridotite, pyroxenite, and eclogite xenoliths have X-ray diffraction patterns and Raman spectra characteristic of highly crystalline graphite of high-temperature origin and are interpreted to have crystallized from C-H-O fluid in the mantle lithosphere beneath cratons. *Watson et al*. [2010] recently investigated the influence of carbon impurities on the bulk electrical conductivity of polycrystalline olivine. A series-type grain boundary impedance in the sample implied a disconnected graphite film on the olivine grain boundaries because of the small amount (~0.16 vol %) of graphite. Subsequently, *Wang et al*. [2013] applied thin disk-shaped morphology to explore the role of graphite on the electrical conductivity in olivine-rich aggregates through the transformation of diamond to graphite. They proposed that graphite can significantly enhance the electrical conductivity in these aggregates if the volume fraction of graphite exceeds ~1.6 vol % (1.0 wt %). In *Wang et al*.'s [2013] experiment, the initial carbon content was extremely high (8 vol % diamond). However, the average carbon concentration in the upper mantle is only about 16–500 ppm [*Deines*, 2002; *Hirschmann and Dasgupta*, 2009], and carbon has a limited phase stability field (depends on P, T, and fO_2) in the upper mantle [*Frost and Wood*, 1997; *Frost and McCammon*, 2008; *Day*, 2012]. Therefore, the electrical conductivity of olivine aggregates containing an unrealistic amount of graphite may not reflect the real electrical properties in the Earth's upper mantle. In contrast, *Yoshino and Noritake* [2011] studied the connectivity of graphite films on the grain boundary of silicate minerals under lower crustal conditions (1 GPa, up to 1273 K), and found that the thinner graphite film (less than 80 nm) on an artificial grain boundary between two quartz crystals is readily destroyed by higher interfacial energy. However, the effect of interfacial energy on the connectivity of graphite film on an olivine grain boundary under upper-mantle conditions has not been investigated.

To examine the connectivity of graphite film at higher temperature and pressure, we performed in situ electrical conductivity measurements at 1 or 3 GPa for two systems: polycrystalline olivine mixed with graphite and olivine bicrystals coated with carbon on their grain boundaries. Such experimental investigations are crucial to verify the validity of graphite hypothesis and to elucidate the origin of high-conductivity anomalies in the lithospheric mantle.

2. Experimental Procedures

The two types of samples (i.e., polycrystalline olivine mixed with graphite and carbon-coated olivine bicrystals) were used to measure the electrical conductivity. The samples of carbon-bearing polycrystalline olivine

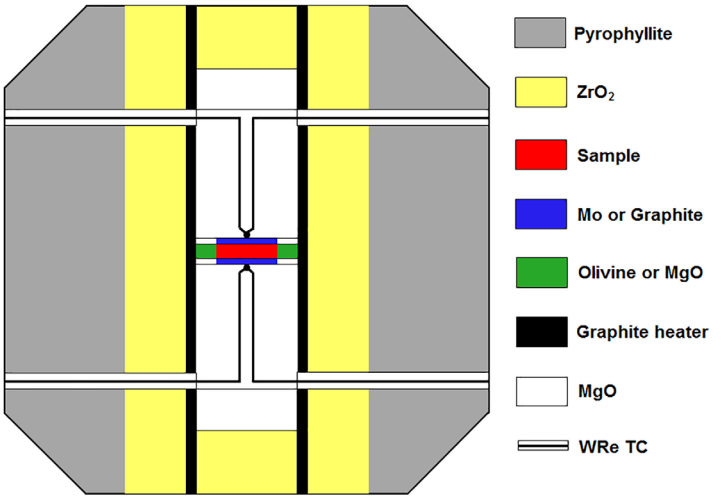

Figure 1. Schematic cross section of cell assembly for conductivity measurement in the DIA-type apparatus.

were prepared by mixing the powders of San Carlos olivine, $(Mg_{0.9}Fe_{0.1})_2SiO_4$, and reagent-grade graphite (0.8 vol %). The average grain size for olivine and graphite are ~5 and 2 μm, respectively. Before weighing, each of the starting powders was dried at 473 K for 24 h in a vacuum oven to remove the absorbed water. Then, these powders were mixed and ground in an agate mortar for more than 3 h. The powder samples of olivine and graphite mixture were placed into a molybdenum capsule and sintered in an end-loaded piston-cylinder apparatus at a pressure of 1 GPa and a temperature of 1523 K with 3/4″ pressure assemblies. The Mo capsule was used to buffer oxygen activity at Mo-MoO_2 (MMO) equilibrium. MMO buffer was often considered to be close to that of iron-wüstite (IW) [*Xu et al*., 2000; *Yoshino et al*., 2006]. In fact, previous studies have demonstrated that graphite can be stably present even under quartz-fayalite-magnetite (QFM) buffer condition, which is distinctly higher oxidation state than IW buffer [*Frost and Wood*, 1997; *Frost and McCammon*, 2008]. Therefore, Mo capsule can assure graphite stability. For the carbon-coated olivine bicrystals, the method for sample preparation was the same as that adopted by *Yoshino and Noritake* [2011]. The sample was a disk with a diameter and thickness of 2 and 1 mm, respectively. The disk was cored from San Carlos single-crystal olivine parallel to the *b* axis. The cored disks were cut into two halves with an arbitrary face normal to the cylindrical axis. The cutting surfaces were polished with diamond paste, and then carbon coating was performed on the polished surfaces with a thickness ranging from several to more than 100 nm.

High-pressure and high-temperature experiments were conducted in a DIA-type apparatus installed at IPM, Okayama University. Figure 1 shows the cell assembly for in situ electrical conductivity measurement. The sample was placed in a San Carlos single-crystal olivine (bored along the *b* axis) or MgO capsule, through which the sample was insulated from the graphite heater and sandwiched by two graphite or Mo electrodes with a diameter and thickness of 2 and 0.5 mm, respectively. Graphite or Mo electrode serves to control oxygen fugacity close to C-CO (CCO) or Mo-MoO_2 (MMO) buffer during conductivity measurements. Although MMO buffer is lower than that of CCO buffer, previous conductivity measurements on carbon-coated quartz reported similar results under both buffers conditions [*Yoshino and Noritake*, 2011].

Electrical conductivity measurements were performed at 1 GPa for a sample of polycrystalline olivine mixed with graphite and at 3 GPa for samples of carbon-coated olivine bicrystals, respectively, using a Solartron 1260 Impedance/Gain-Phase Analyzer (combined with a Solartron 1296 Interface if the sample resistance was higher than MΩ) at conditions of $T = 300$–1700 K (Table 1). The complex impedance spectra were obtained over frequencies ranging from 10^6 to 10^{-1} Hz under AC voltage with an amplitude of 1 V. The experimental strategy for electrical conductivity of the sample containing carbon was as follows. (1) The sample was compressed to the desired pressure. (2) In the first cycle, the electrical conductivity of the sample was measured at 100 K interval until the sample was heated up to the target temperatures (1500, 1600, and 1700 K). (3) The sample was annealed at the maximum temperature, and the conductivity was frequently monitored to detect the stability of graphite film on the grain boundary as a function of annealing time (from 3 to 66 h). Then, the samples were cooled to 500 K, and the conductivities were measured at an interval of 50 K each. (4) The samples were reheated to the highest temperatures in the second cycle to check the reproducibility of the conductivity measurements. Then, the impedance spectra were obtained at a step of 50 or 100 K as temperature decreases to 500 K (the second cooling path). For the carbon-coated sample, the initial coated carbon layer on the olivine grain boundary was amorphous carbon, which would

Table 1. Summary of Experimental Conditions

Run No.	Sample[a]	Electrode	Capsule[b]	P (GPa)	T_{max} (K)	Log σ_0 (S/m)	ΔH (eV)	Duration (h)[c]	d (nm)[d]	Remarks
A2532	Olivine aggregate	Mo	MgO	1	1700	3.25 ± 0.18	1.62 ± 0.04			
A2534	Olivine + 0.8 vol %C	Mo	MgO	1	1700	2.46 ± 0.33	1.32 ± 0.07	5		
A2542	C-coated	Graphite	SC olivine	3	1700	1.09 ± 0.01	0.03	66	178	
A2543	C-coated	Mo	SC olivine	3	1500	2.85 ± 0.07	1.58 ± 0.02	10	2	
A2552	C-coated	Graphite	MgO	3	1600	1.81 ± 0.14	1.55 ± 0.03	11	25	
A2553	C-coated	Graphite	MgO	3	1600	-0.61	0.01	3	65	First cooling
						2.24 ± 0.07	1.46 ± 0.02	33		Second cooling
A2554	C-coated	Graphite	SC olivine	3	1600	0.32 ± 0.01	0.01	19	140	First cooling
						2.97 ± 0.11	1.30 ± 0.03	27		Second cooling
A2555	C-coated	Graphite	MgO	3	1600	0.97	0.03	48	153	
A2556	Olivine[b]	Mo	MgO	3	1700	2.43 ± 0.14	1.57 ± 0.03			
A128[e]	Graphite	Mo	MgO	1	1273	5.17	0.02			

[a]C-coated means sample is carbon-coated single-crystal San Carlos olivine which was cut parallel to *b* axis.
[b]SC olivine denotes the capsule material is single-crystal San Carlos olivine bored along *b* axis.
[c]Annealing time (h) at the maximum temperature.
[d]Thickness (d_{film}) of graphite film was calculated from the approach adopted by *Yoshino and Noritake* [2011], where $d_{film} = \frac{\pi r R_{graphite}}{2R_{film}}$, r is radius of olivine (=1 mm), $R_{graphite}$ is the resistance of graphite, R_{film} is the resistance of graphite film at the maximum temperature.
[e]This results from reference [*Yoshino and Noritake*, 2011].

crystallize to graphite during the first heating. After the conductivity measurement, the recovered samples were observed by scanning electron microscope (SEM) and optical microscope to evaluate the connectivity of the graphite film on the grain boundary.

Nine experiments were performed for the two types of samples at various temperatures and pressure ranges (Table 1). The conductivities of polycrystalline olivine and San Carlos single-crystal olivine parallel to the *b* axis were also measured at 1 and 3 GPa, respectively, and at a temperature of up to 1700 K to determine the lower bounds of the polycrystalline olivine mixed with graphite and carbon-coated olivine bicrystals. The upper bound corresponding to the conductivity ($\sim 10^{5.17}$ S/m) of graphite was determined by *Yoshino and Noritake* [2011]. The electrical conductivity measurements were performed along the heating-cooling cycle. The impedance spectra were fitted by a single parallel RC equivalent circuit to determine the sample resistance. The sample conductivity and the thickness of the graphite film on the grain boundary were calculated from the minimum resistance at the maximum annealing temperature and the sample dimensions.

Dihedral angle measurement is another effective way to evaluate the interconnection of graphite in olivine matrix if the system has established textural equilibrium. For the olivine-graphite aggregate, after conductivity measurement, a polished section of the sample was vacuum-impregnated with epoxy to minimize the plucking of grains. The cross section was finally polished by diamond paste. Microscopic observations were made through secondary electron images (SEI) and backscattered electron images (BEIs). Dihedral angle measurements were performed on photographs with magnifications $\geq$1000×. More than 100 measurements were performed in the cross section for the recovered sample. The true dihedral angle was estimated from the median of the distribution of the apparent angles [*Jurewicz and Jurewicz*, 1986].

3. Results

3.1. Carbon-Bearing Sample

The electrical conductivity of rocks containing secondary conductive phases (i.e., graphite, fluid, melt, etc.) depends primarily on the electrical conductivity of the secondary phases and on their geometry along grain boundaries, if the dominant phase is less conductive. The impedance spectroscopy measurement is an effective approach to identify the influence on secondary conductive phase on bulk conductivity. In general, in the case of the presence of an interconnected highly conductive pathway, the circuit was composed of the response of the less conductive grain interior and conductive secondary phase in a parallel circuit. Conversely, in the absence of an interconnected highly conductive pathway, the circuit was composed of the response of the grain interior and isolated conductive phase in a series circuit. In this case, one arc derived from secondary conductive phase with RC parallel circuit is completely masked by that derived from less conductive phase because of huge (orders of magnitude) resistance contrast [*Yoshino*, 2010]. Therefore, the

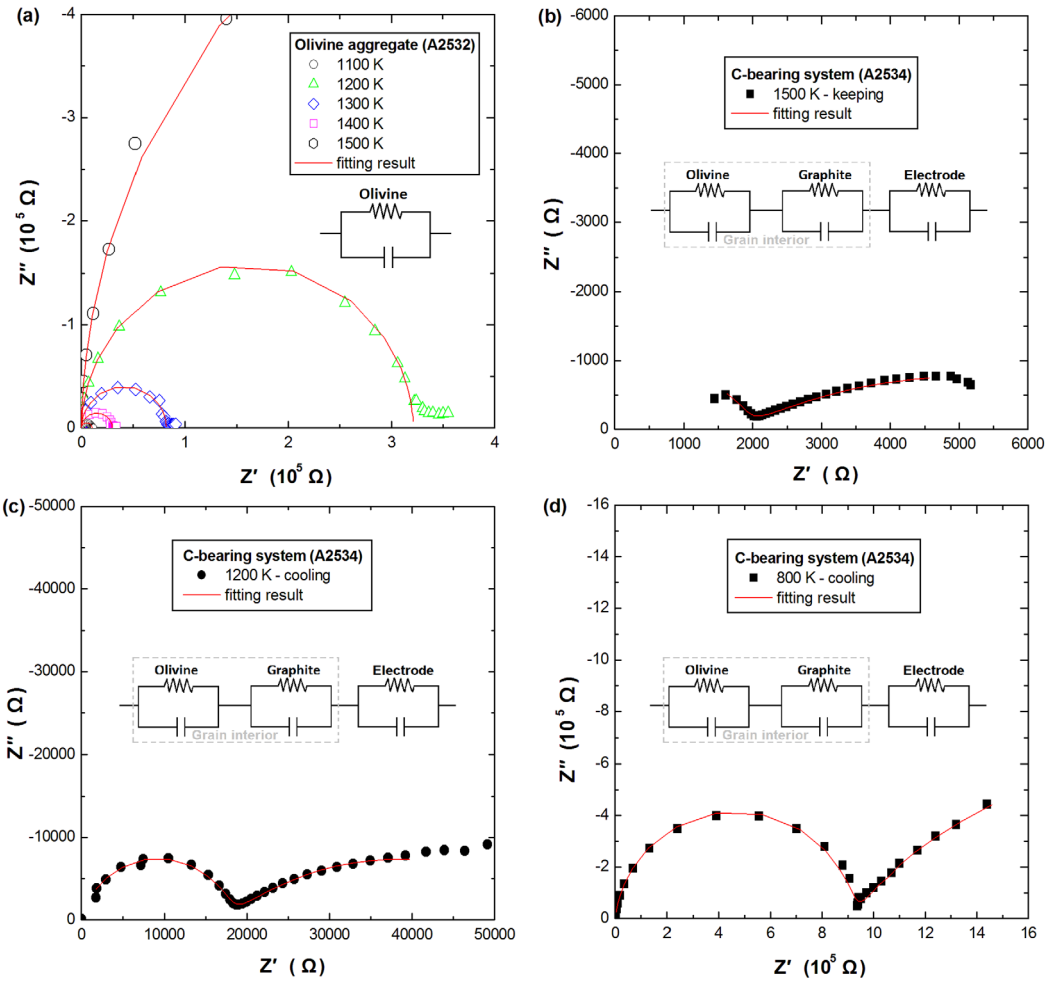

Figure 2. The representative impedance spectra of the carbon-bearing sample acquired at cooling path and the equivalent circuit. (a) Olivine aggregates (A2532) are fitted with a single R-CPE circuit element. (b–d) Typical impedance spectra of the carbon-bearing sample (A2534) acquired at different temperature in the second cooling cycle. Note that the raw data can be well fitted by the equivalent circuit, which is composed of two R-CPE parallel circuits connected in series.

first arc appeared in Nyquist diagram was considered to be equal to the sample resistance. *Watson et al.* [2010] observed three impedance arcs in the complex impedance plane from a carbon-bearing sample at 1 GPa, and interpreted them as grain interior (first arc), grain boundary (second arc), and electrode reaction mechanism (third arc) from high to low frequency, respectively. However, the presence of the second arc in low frequency range has not been observed for carbon-bearing system in this study and previous investigations [*Roberts et al.*, 1999; *Yoshino and Noritake*, 2011; *Wang et al.*, 2013]. Thus, the low frequency tail is probably due to sample-electrode interface effects [*Roberts et al.*, 1999; *Yoshino and Noritake*, 2011].

The representative impedance spectra for carbon-free and carbon-bearing samples, their associated fits and equivalent circuits, are illustrated in Figure 2. The spectra for carbon-free olivine aggregate can be well fitted by an equivalent circuit consisting of one resistance-constant phase element (R-CPE) circuit element [*Barsoukov and Macdonald*, 2005] (Figure 2a), suggesting grain interior mechanism is dominant. In the carbon-bearing sample (A2534), the impedance spectra showed a semicircle at high frequencies and an additional part (tail) at low frequencies (Figures 2b–2d). Remarkably, the decreasing temperature resulted in the increase of the impedance arc radius and arc becomes a completely semicircle at low temperature, which can be well fitted by an equivalent circuit consisting of two R-CPE circuit elements (one is grain interior, and another is polarization between electrode-sample) in a series circuit. However, the additional "tail" decreases with decreasing temperature, implying that the sample-electrode interface effect becomes smaller at low temperature.

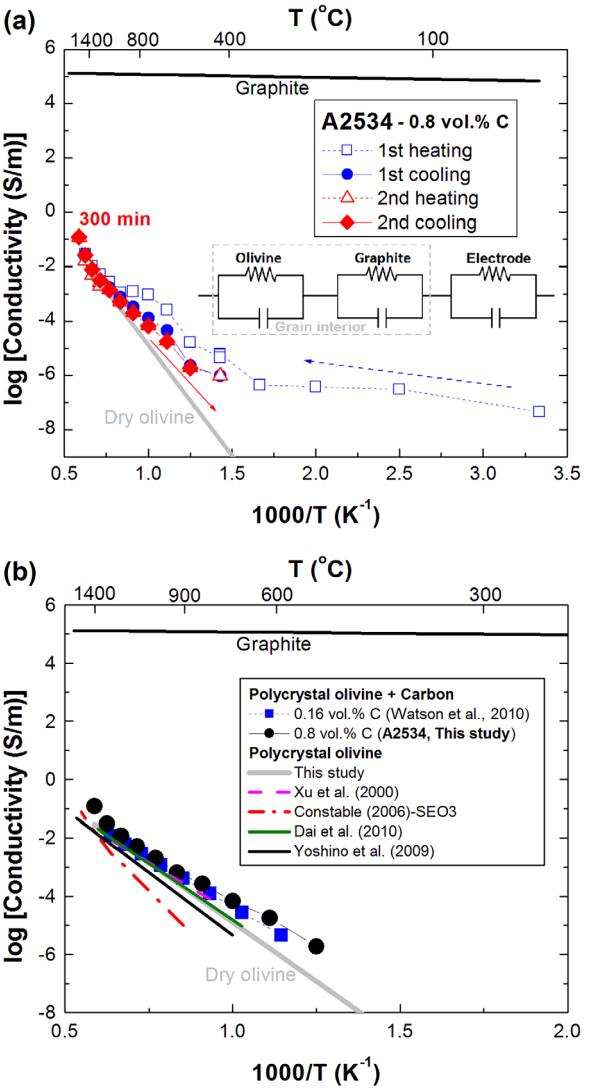

Figure 3. Arrhenius plots of the electrical conductivity for carbon-bearing olivine system at 1 GPa. (a) Electrical conductivity of polycrystalline olivine mixed with graphite as a function of reciprocal temperature (Run A2534). Open squares and closed circles denote results of the first and second heating-cooling cycles, respectively. Thick line denotes the electrical conductivity of graphite [*Yoshino and Noritake*, 2011]. Light gray line indicates the electrical conductivity of dry olivine aggregate (Run A2532). (b) Summary of the experimental results. Note that, a comparison of the present laboratory conductivity of dry olivine with previous studies [*Xu et al.*, 2000; *Constable*, 2006; *Yoshino et al.*, 2009; *Dai et al.*, 2010] is also shown in Figure 3b.

Figure 3a shows a result of electrical conductivity measurement for polycrystalline olivine mixed with graphite. The electrical conductivity values increased with the temperature from 300 K to the highest temperature. The first cooling and second heating paths showed reproducibility. When reheating to the maximum temperature (1700 K) in the second cycle, the sample was annealed for 5 h at 1700 K, in which the conductivity was nearly constant. The conductivities were very close to those of dry polycrystalline olivine in the cooling path, which displayed a linear relationship in the logarithmic conductivity versus reciprocal temperature (Figure 3a). Thus, an equivalent circuit could be considered a series RC circuit composed of olivine and isolated graphite, implying that graphite cannot be interconnected in olivine matrix.

The activation enthalpy and pre-exponential factor were calculated using the Arrhenius equation:

$$\sigma = \sigma_0 \exp(-\Delta H/kT), \quad (1)$$

where σ_0 is the pre-exponential factor, ΔH is the activation enthalpy (eV), k is the Boltzmann constant, and T is the absolute temperature. The pre-exponential factor and the activation enthalpy were determined by the least square fitting of the data to the Arrhenius equation. The resultant parameters are summarized in Table 1. The BEIs of the run products showed that grain growth occurred when they were annealed at a high temperature. The average size of the olivine crystal was approximately 10–15 μm (Figure 8a). The graphite was isolated in the grain corners rather than interconnected film on grain boundaries.

Previous studies indicated that the presence of a small amount of conductive impurities can enhance conductivity [*Glover*, 1996; *Roberts et al.*, 1999; *Yoshino et al.*, 2003, 2004; *Watson et al.*, 2010], once such conductive phase is connected in some ways (interconnected film or tubular structure). However, the present experimental results showed that the effect of graphite on the electrical conductivity of olivine aggregates is very small (Figure 3b) when the fraction of graphite is 0.8 vol %. On the contrary, the large activation enthalpy of polycrystalline olivine mixed with graphite (1.32 eV) obtained in the present study (Table 1) is rather close to that of olivine (1.62 eV), suggesting that the graphite is disconnected at high temperature. Figure 3b also shows the comparison of the electrical conductivity of olivine aggregate in the present study with that of previous studies. Our results agree well with those reported by previous studies at high pressure [*Xu et al.*, 2000; *Yoshino et al.*, 2009; *Dai et al.*, 2010]. However, these results are higher than those of the SEO3 model [*Constable*, 2006].

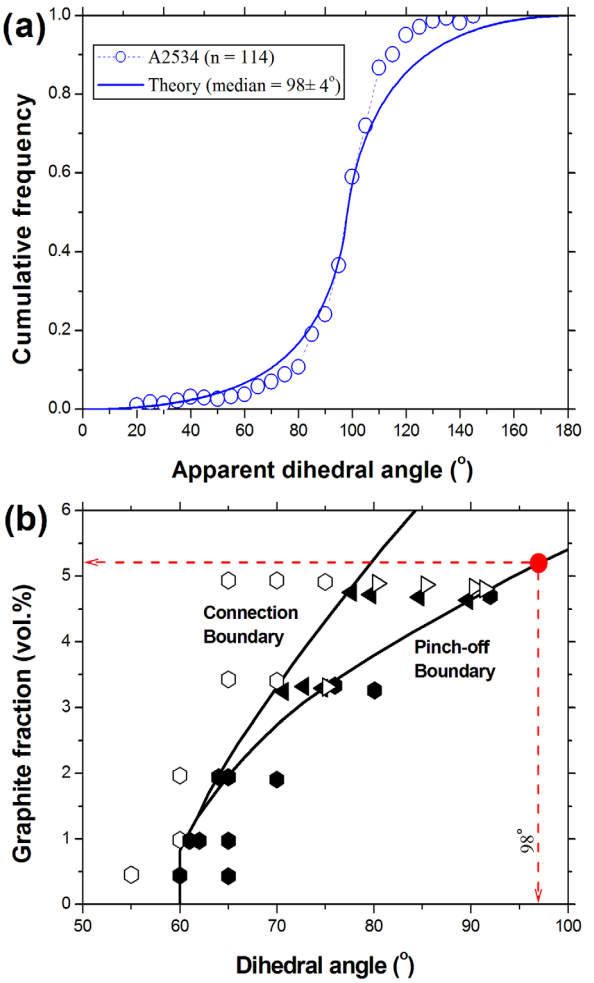

Figure 4. (a) Comparison of theoretical and measured distributions of apparent dihedral angle for graphite/olivine system. (b) Graphite pinch off and connection conditions in dihedral angle versus graphite fraction [modified after *von Bargen and Waff*, 1986]. The black open and closed symbols are from *von Bargen and Waff* [1986]; the red closed circle is from the present study.

The result of the dihedral angle measurement (with 0.8 vol %) is shown in Figure 4a. The median angle from the distribution of the apparent angles is approximately 98° in the olivine/graphite system. This observation implies that the percolation threshold for graphite is more than 5 vol % (Figure 4b) once the graphite grains are interconnected. However, the cumulative frequencies for the dihedral angle distribution measured on the 2-D section show a good fit for the theoretical cumulative frequency curve (Figure 4a), suggesting that the system nearly establishes the textural equilibrium.

3.2. Carbon-Coated Samples

Figure 5 shows two typical examples of electrical conductivity measurements for carbon-coated samples. In run A2554 with ~140 nm film (Figure 5a), the sample conductivity slightly increased with temperature in the first heating path. At the beginning of annealing at 1600 K, the sample conductivity was three orders of magnitude higher than the single-crystal olivine conductivity. Figure 6 shows the representative impedance spectra of the carbon-coated systems during heating path and annealing at the highest temperature. The impedance spectra showed a complete semicircular at high frequencies and an additional part (tail) at low frequencies. The increasing temperature resulted in the decrease of the impedance arc radius (Figure 6a). Finally, the first arc disappeared completely, and a line appeared in positive Z'' as a result of the dominance of the wire induction [*Gaillard et al.*, 2008; *Pommier et al.*, 2010; *Ni et al.*, 2011] at the beginning of the annealing temperature (Figure 6b). The conductivity decreased by one order of magnitude after heating at 1600 K for 19 h (Figures 5a and 6b). The conductivity values were nearly independent of the temperature along the first cooling and second heating paths. This small temperature dependence ($\Delta H = 0.01$ eV) is similar to that of graphite ($\Delta H = 0.02$ eV), which means that the graphite film is still interconnected on the olivine grain boundary, and the sample conductivity is controlled by the conductive phase (graphite) in a parallel RC circuit. The temperature was maintained at 1600 K after the second cycle. The sample conductivity showed a large drop (approximately two orders of magnitude). The corresponding impedance spectra are displayed in Figure 6c. As a result, the sample conductivity was close to the conductivity of the single-crystal olivine parallel to the *b* axis, and the activation enthalpy of a bulk sample (1.55 eV) was nearly the same as that of olivine crystal (1.57 eV). This behavior implies that the graphite film is disconnected on the olivine grain boundary, and the bulk conductivity is controlled by the resistive phase (olivine matrix) in a series RC circuit. The relationship of conductivity-temperature-time for the carbon-coated sample (run A2554 ~140 nm) observed in the present study (Figure 5a) is the same as that for the carbon-coated quartz bicrystal system reported by *Yoshino and Noritake* [2011]. The time variation of impedance arc (Figure 6) should reflect a change of conduction mechanism from a parallel RC circuit to a series one, suggesting a textural transition from an interconnected graphite film to a disconnected one. Therefore, the graphite film on the olivine grain boundary is not stable at high temperature.

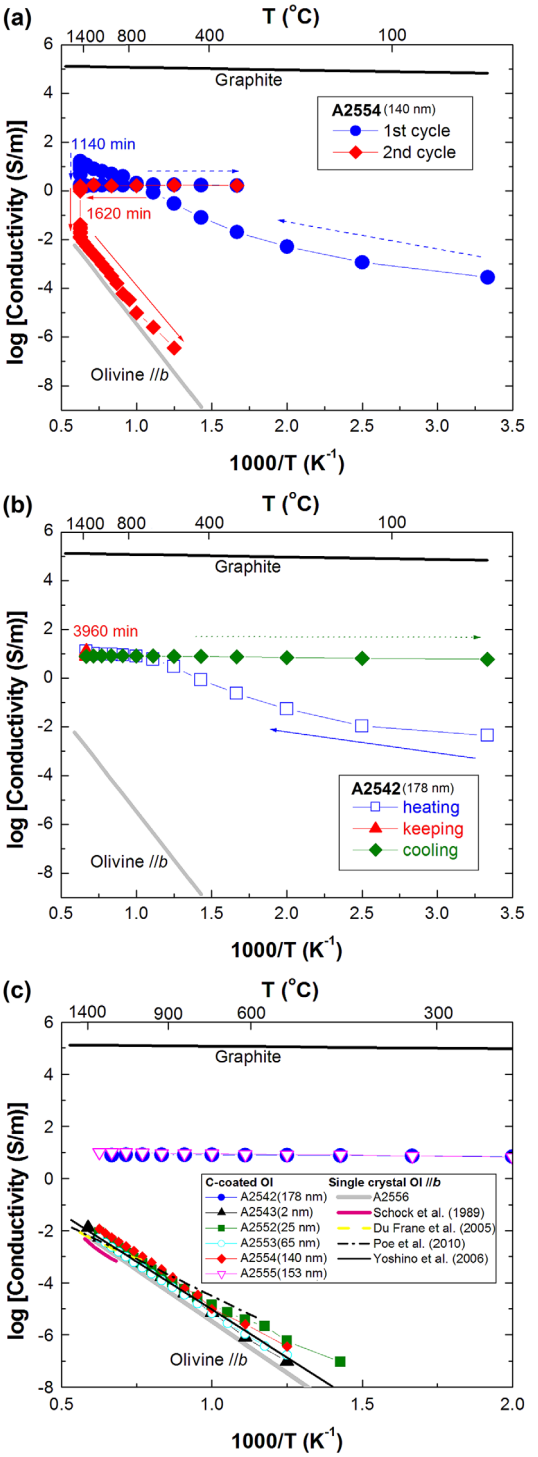

Figure 5. Arrhenius plots of the electrical conductivity for carbon-coated olivine bicrystals system at 3 GPa. (a) Electrical conductivity of the sample with thinner graphite film (Run A2554 ~ 140 nm) as a function of reciprocal temperature. Closed circles and diamonds denote results of the first and second heating-cooling cycles, respectively. (b) Electrical conductivity of the sample with the thickest graphite film (Run A2542 ~ 178 nm) as a function of reciprocal temperature. Open squares, closed triangles and diamonds denote the first heating, keeping and cooling paths. (c) Summary of the experimental results for carbon-coated olivine bicrystals samples. Note that, a comparison of the present laboratory conductivity of San Carlos olivine single crystal with previous studies [*Schock et al.*, 1989; *Du Frane et al.*, 2005; *Yoshino et al.*, 2006; *Poe et al.*, 2010] is also shown in Figure 5c. Thick line denotes the electrical conductivity of graphite [*Yoshino and Noritake*, 2011]. Light gray line indicates the electrical conductivity of San Carlos olivine single-crystal parallel to *b* axis (Run A2556).

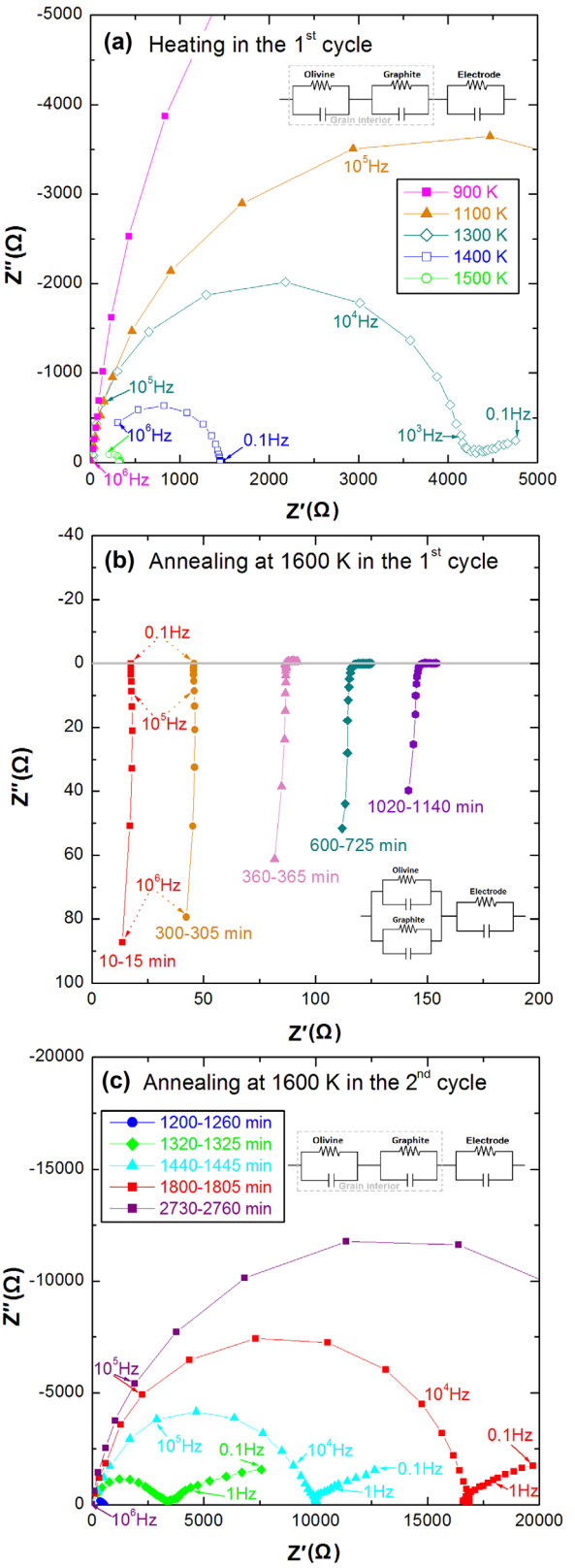

Figure 6. Evolutions of representative impedance spectra of the carbon-coated olivine bicrystals system (run A2554 ~ 140 nm) with temperature and time. (a) Impedance spectrum in the first heating. (b) Annealing at 1600 K in the first cycles. (c) Annealing at 1600 K in the second cycles.

In run A2542, which had a thicker carbon film of ~178 nm (Figure 5b), the conductivity values were initially high and slightly increased with the temperature during heating to the target temperature (1700 K). The sample was annealed for a relatively long duration (66 h) at the maximum temperature. However, the change in the sample conductivity with time was small, which was at least three orders of magnitude higher than that of the single-crystal olivine. In the cooling path, the conductivity values were nearly independent of temperature, and the small temperature dependence ($\Delta H = 0.03$ eV) was similar to that of graphite conductivity ($\Delta H = 0.02$ eV). These observations indicated that the interconnection of graphite film on the olivine grain boundary was maintained and not completely broken via annealing at a high temperature.

A summary of the experimental results of the conductivity measurements for carbon-coated systems is shown in Figure 5c. The conductivity for most runs in the last cooling path was very close to that of a single-crystal olivine parallel to the *b* axis. This observation suggests that the interconnectivity of the graphite film on the olivine grain boundary is destroyed during annealing at high temperature, except for the two runs (i.e., A2542 and A2555), with a thick graphite film showing relatively high conductivity (~10^1 S/m).

Given that the stability (interconnection or disconnection) of a graphite film is controlled by interfacial energy [*Yoshino and Noritake*, 2011], the annealing time kept at the maximum temperature varies with the decreasing rate in electrical conductivity. Figure 7 shows a systematic variation of the absolute conductivity values for carbon-coated samples as a function of time during annealing at the maximum temperature. All samples finally showed a decrease in conductivity after a certain time passed. The conductivity of the sample with the thinnest film (2 nm) annealed at 1500 K showed a rapid decrease within 1 h. However, the conductivity of the sample with the thickest film (178 nm) annealed at 1700 K slightly increased at the beginning of the annealing and then became constant. The conductivity of the samples started to decrease after heating for more than 2 days because of the onset of the destruction of

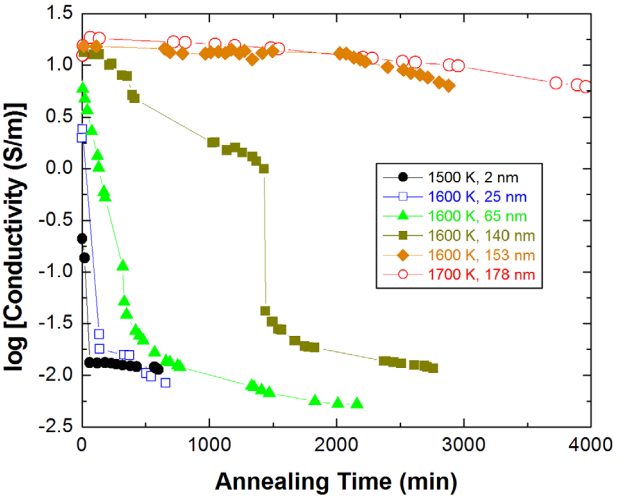

Figure 7. Systematic variation of the absolute conductivity values for carbon-coated samples with various thickness of graphite films as a function of time during annealing at the maximum temperature. All samples finally showed a decrease of conductivity after a certain time passed.

interconnectivity within the graphite film. However, the absolute decrease rate was very slow. In this study, the conductivity decrease rate could be defined by a slope in Figure 7 after the conductivity reached the maxima. The time required to start decreasing sample conductivity was controlled by the rate of decrease in conductivity, whereas the decrease rate mainly depended on the thickness of the graphite film rather than on temperature. The absolute decrease rate decreased with increasing graphite film thickness. This finding suggests that the sample with a thick graphite film needs a long time to destroy interconnectivity.

To evaluate the connectivity of the graphite film after the conductivity experiment, the microstructures of the recovered samples were examined with SEM for carbon-bearing systems and optical microscope for carbon-coated systems across the olivine grain boundary. As shown in Figure 8a, the graphite located at the grain corner of the olivine crystal was isolated in the olivine matrix. It did not form an interconnected film on the olivine grain boundaries. The round shape of the olivine grain with small grain size ($\sim$10 μm) suggests that the present experiments attained textural equilibrium.

The olivine grain boundary in the carbon-coated systems, as depicted in Figure 8b, for the run A2542 (graphite film $\sim$178 nm) characterized with high conductivity (Figure 5b) was mostly covered with a graphite film. The grain shape at the interface was round, and substantive clustering of graphite was present. Although the graphite film on the olivine grain boundary was still interconnected for the sample with the thickest film (Figure 8b), the experimental duration was extremely short compared with geological time. Therefore, the graphite film on the olivine grain boundary is expected to be finally broken due to the higher interfacial energy. In contrast, the distribution of graphite for the sample (run A2554) showing low conductivity after annealing (Figure 5a) is isolated at the interface, and most graphite grains have a globular morphology (Figure 8c). These textural observations are similar to those observed in a quartz grain boundary [*Yoshino and Noritake*, 2011]. This finding implies that the interconnectivity of thin graphite film on the olivine grain boundary is destroyed at a high temperature.

4. Discussion

4.1. Comparison With Previous Studies

Our data on the electrical conductivity of carbon-bearing and carbon-coated systems are compared with the previous results (Figure 9). *Watson et al*. [2010] performed the electrical conductivity measurements of polycrystalline olivine containing a small amount ($\sim$0.16 vol %) of graphite as the function of temperature at 1 GPa. They found that the conductivity values of the carbon-bearing olivine aggregate are very close to those of olivine because of the isolated distribution of graphite on the olivine aggregate (Figure 9a). This observation agrees well with the present result. *Wang et al*. [2013] investigated the influence of graphite on the electrical conductivity of olivine aggregates within the temperature range of 1173–1673 K at 4 GPa. However, their data, showing very high conductivity and small temperature dependence, are completely inconsistent with our data and those of the previous study [i.e., *Watson et al*., 2010]. Their data also have a similar activation enthalpy (0.04–0.16 eV) of the graphite conductivity. This inconsistency can be mainly caused by the different starting materials. In our carbon-bearing experiment and that of Watson et al., graphite was directly used as the starting material to measure electrical conductivity. However, in the study by Wang et al., a diamond was used as the starting carbon source, and then olivine aggregates containing diamond were annealed in the stability field of graphite. Thus, the phase transformation from diamond to

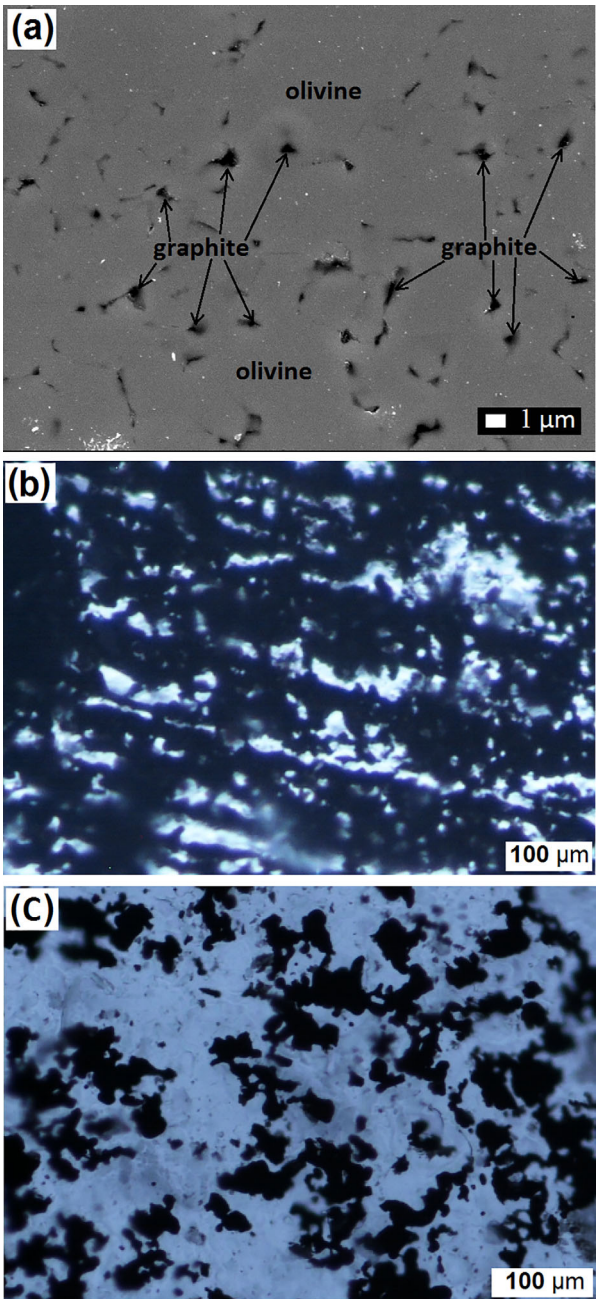

Figure 8. Microstructural observations of recovered samples. (a) Back-scattered electron image (BSE) of olivine mixed graphite sample (A2534). (b) Transmitted light image of sample (run A2542) across the olivine grain boundary indicating high conductivity. (c) An image of sample (run A2554) indicating low conductivity similar to single-crystal olivine. Note that these two transmitted light images were taken perpendicular to the grain boundary and focused in the plane of the grain boundary.

graphite quickly occurred during heating. The thermal expansion coefficient of graphite is considerably larger than that of diamond at high temperatures [*Zhao and Spain*, 1989; *Day*, 2012]. Owing to the very high volume fractions (4–7 vol %) of carbon in *Wang et al.*'s [2013] experiment, graphite transformed from diamond may have formed the interconnected film on the olivine grain boundary at the initial stage of the phase transformation because of its large volume expansion. In addition, compared with a long annealing duration including several heating-cooling cycles in our conductivity experiments, their short annealing time is not enough to break the thick graphite film, as depicted in Figure 7.

The run products of the carbon-bearing system show the rounded morphology and isolated feature at the olivine grain corner (Figure 8a), which are completely different from the disk shape along the olivine grain boundary observed by *Wang et al.* [2013]. This observation indicates that the huge anisotropy in the surface energy does not contribute to the development of the anisotropic distribution of graphite when graphite is used as the starting material. After the phase transformation, the textural evolution is controlled by the interfacial energy minimization in the olivine/graphite system. Their run duration is not enough to evaluate this process.

Yoshino and Noritake [2011] measured the electrical conductivity of graphite films on the synthetic grain boundaries of quartz bicrystals at 1 GPa and at temperatures up to 1200 K. Their results showed that the interconnection of the graphite film is readily destroyed on the quartz grain boundaries under the lower crustal condition when the film was thin ($<$80 nm). In most cases, the final conductivity values of the graphite film are equivalent to those of a single-crystal quartz. No direct experimental data on carbon-coated olivine bicrystals are available, as shown in Figure 9b. Thus, the present results measured under the upper-mantle conditions were compared with the data from *Yoshino and Noritake* [2011]. Although the present experimental conditions (3 GPa and up to 1700 K) for carbon-coated olivine largely differ from those (1 GPa and up to 1200 K) of the quartz system [*Yoshino and Noritake*, 2011], the electrical behaviors between the two systems are nearly the same. These characteristics imply that the graphite films are not stable in the major silicate minerals in terms of interfacial energy minimization.

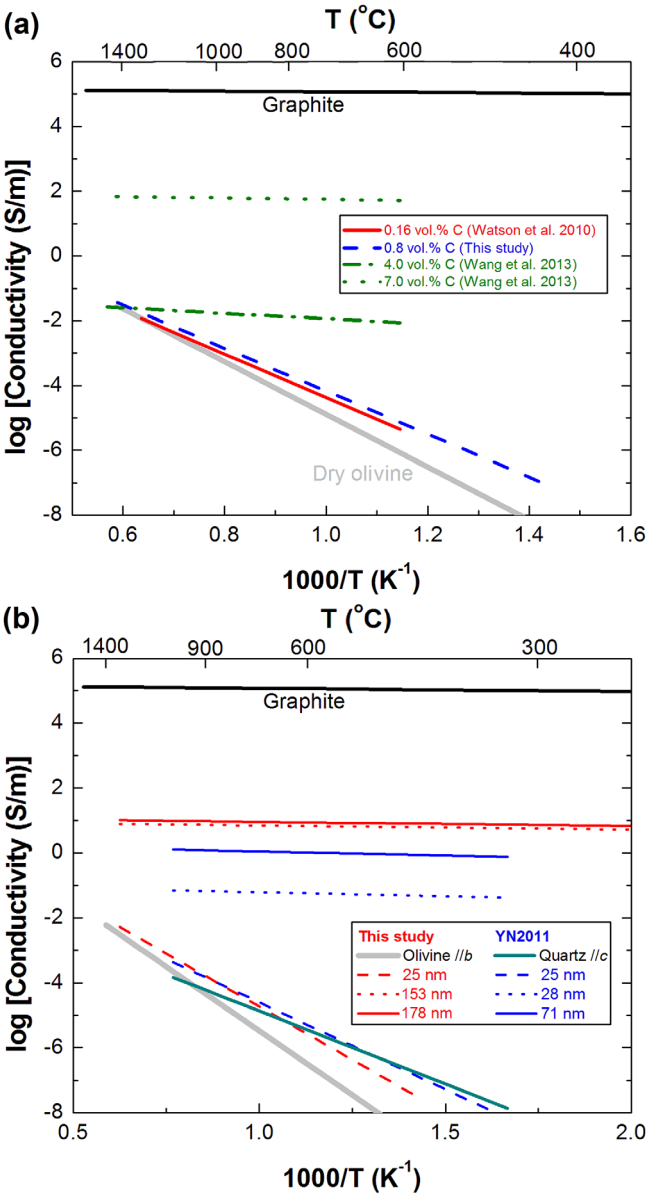

Figure 9. Comparison of results for electrical conductivity of carbon-bearing olivine aggregates (a) and carbon-coated olivine bicrystals (b) systems under upper-mantle conditions. YN2011—*Yoshino and Noritake* [2011].

A dramatic decrease in conductivity during the conductivity measurement may occur through graphite oxidation during annealing. However, we confirmed the presence of graphite on the olivine grain boundary even if the duration time was more than 2 days at 1700 K and no evidence for the presence of C-O-H fluid was found (Figure 8). Usually, Carbon-fluid buffered equilibria are close to the quartz-magnetite-fayalite (QFM) buffer [*Watson and Brennan*, 1987]. In the present study, the oxygen fugacity was controlled by the Mo-MoO_2 buffer or a C-CO buffer. Previous investigations demonstrated that both buffers yield similar results, and graphite can be stably present at high-T/fO_2 conditions [*Frost and Wood*, 1997; *Frost and McCammon*, 2008]. Thus, the decrease in conductivity of the carbon-coated olivine bicrystal should be caused by the destruction of the interconnected graphite film, but not by carbon volatilization.

4.2. Effects of Temperature, Annealing Time, and Graphite Film Thickness on Interconnection of Graphite

The weak temperature dependence of the electrical conductivity of graphite means that effective bulk conductivities also vary slightly with temperature if graphite controls the bulk conductivity. This point is proven for carbon-bearing and carbon-coated systems in the present study, as shown in Figures 5 and 9b. On the contrary, the activation enthalpy determined along the final cooling path is high and close to that of silicate minerals if the connectivity of graphite is broken during conductivity measurements. In such a circumstance, a strong temperature dependence on the sample bulk conductivities is expected (Figures (3 and 5), and 9).

The decrease in electrical conductivity with time (rate of decrease in conductivity) for carbon-coated olivine bicrystal during annealing at a high temperature depends on the thickness of the graphite film rather than on temperature (Figure 7). This observation disagrees with the previous investigation in carbon-coated quartz bicrystal [*Yoshino and Noritake*, 2011], which shows that the conductivity decrease rate is apparently constant at the same temperature and increases with increasing temperature. This discrepancy may be caused by the different temperature range for conductivity measurement between the current study and theirs. In the experiment by Yoshino and Noritake, the maximum temperature was relatively low (~1200 K). Thus, the conductivity decrease rate was very sensitive to temperature because the Arrhenian effect intensifies at low temperatures. By contrast, the very high measured temperature in

our study (~1700 K) generates the condition that conductivity decrease rate is considerably sensitive to the thickness of the graphite film but not on temperature. On the contrary, the activation enthalpy for the apparent disconnection rate is calculated as ~24 kJ/mol if the kinetics analysis proposed by *Yoshino and Noritake* [2011] is followed. This finding suggests weak temperature dependence. The activation enthalpy for the apparent disconnection rate of a graphite film on olivine grain boundaries (i.e., ~24 kJ/mol) is close to that for carbon diffusion in olivine grain boundaries [14 kJ/mol; *Hayden and Watson*, 2008]. Therefore, the disconnection of the graphite film is probably controlled via carbon grain boundary diffusion in silicates, but not via self-diffusion of carbon in graphite, as suggested by *Yoshino and Noritake* [2011]. In consideration of the activation enthalpy for carbon self-diffusion in graphite [682 kJ/mol; *Kanter*, 1957], which is higher than that for disconnection kinetics of graphite along the quartz grain boundaries (148 kJ/mol), the interpretation of *Yoshino and Noritake* [2011] is incorrect. The disconnections of the graphite films in both olivine and quartz grain boundaries are prone to be controlled by the grain boundary diffusion of carbon. High diffusion rates for carbon diffusion in olivine grain boundaries [*Hayden and Watson*, 2008] imply that the interconnectivity of graphite is readily destroyed even at low temperatures equivalent to the lithospheric mantle. Therefore, the high-conductive regions of the lithospheric mantle cannot be explained by graphite.

Owing to the huge conductivity contrast between graphite (~10^5 S/m) and silicate minerals (e.g., in olivine $<10^{-2}$ S/m), a small amount of interconnected graphite has been proposed to greatly enhance rock conductivity [*Duba and Shankland*, 1982; *Frost et al*., 1989; *Roberts et al*., 1999]. The present results are compared with those of several conduction models to explain the high-conductive regions in the lithospheric mantle by estimating the interconnection of graphite in a silicate matrix and the amount of carbon content that can produce sufficiently high conductivities. In order to evaluate the effect of graphite fraction on the bulk electrical conductivity, various geometrical models have been proposed, such as the parallel and series models [*Schulgasser*, 1976, 1977], the cube model [*Waff*, 1974], the tube model [*Schmeling*, 1986], the Hashin-Shtrikman upper and lower bound models [*Hashin and Shtrikman*, 1962].

The series and parallel (SP) models give the maximum and minimum conductivity values of two-phase or multiphase systems [*Schulgasser*, 1976, 1977]:

$$\sigma_S = \frac{\sigma_1 \sigma_2}{f_1 \sigma_2 + f_2 \sigma_1} \tag{2a}$$

$$\sigma_P = f_1 \sigma_1 + f_2 \sigma_2 \tag{2b}$$

where σ_1 and σ_2 are the conductivity of two coexisting phases, and f_1 and f_2 are their volume percentages.

Waff [1974] proposed a cube model to describe the bulk conductivity as a function of conductive phase fraction. This model supposed that cubic grains with a low conductivity are all the same size and are surrounded by a high-conductivity phase layer of uniform thickness dependent on conductive phase fraction (ϕ) and that the conductivity of resistive phase is negligibly small. The bulk conductivity is given by

$$\sigma_{bulk} = \left[1 - (1-\phi)^{\frac{2}{3}}\right] \sigma_m \tag{3}$$

where σ_m is the conductivity of conductive phase.

The tube model, proposed by *Schmeling* [1986], represents the cases that conductive phase is not distributed along the grain boundaries, but in a network along the triple junctions. The effective conductivity is given by

$$\sigma_{bulk} = \frac{1}{3}\phi \sigma_m + (1-\phi)\sigma_s \tag{4}$$

where σ_s is the conductivity of resistive phase.

The Hashin-Shtrikman upper (HS+) bound [*Hashin and Shtrikman*, 1962] is a frequently used model to predict the maximum effective bulk conductivity of an interconnected two phase mixture. In this model, the matrix consists of a conductive phase surrounding spherical inclusions with a lower conductivity. The spherical grains are isolated from each other by the conductive phase, so this model is applicable to cases in which conductive phase is distributed along the grain boundaries and filling triple junctions of spherical grains. In the HS+ model, the bulk conductivity is expressed as:

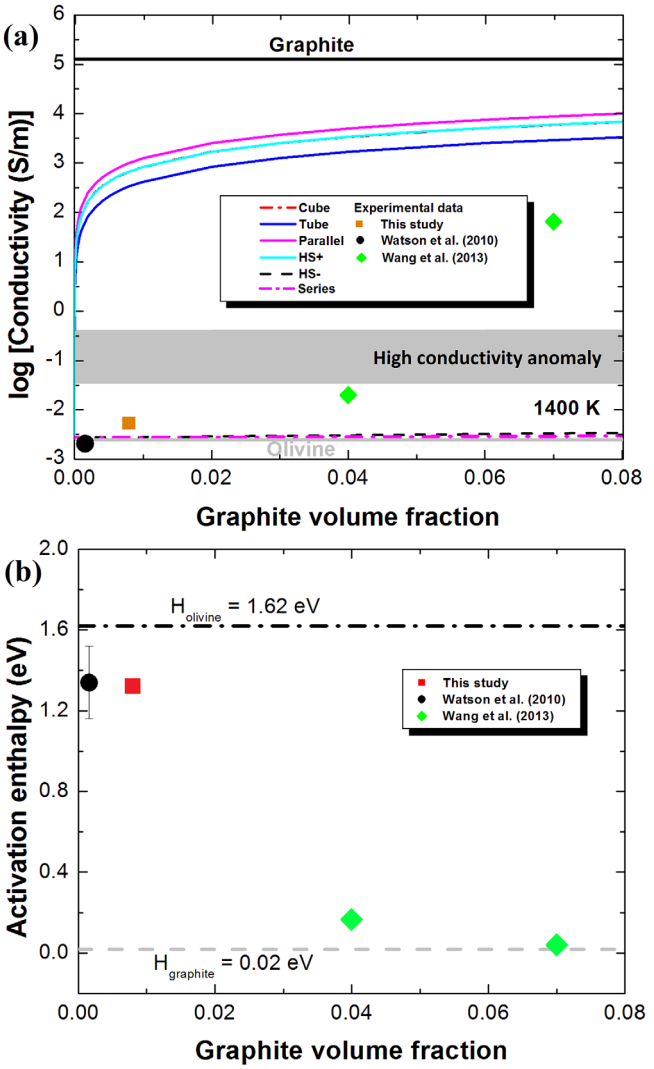

Figure 10. (a) Logarithm of electrical conductivity versus graphite fraction for carbon-olivine rock at 3 GPa and 1400 K according to two-phase mixture. The electrical conductivity of olivine was fixed at $10^{-2.56}$ S/m from this study, graphite was fixed at $10^{5.1}$ S/m [*Yoshino and Noritake*, 2011], respectively. HS^+, Hashin-Shtrikman upper bound; HS^-, Hashin-Shtrikman lower bound [*Hashin and Shtrikman*, 1962]. Shaded region indicates a typical range of conductivity values observed in regions with high-conductivity anomaly of the upper mantle [*Shankland and Waff*, 1977; *Jones et al*., 2003; *Jones et al*., 2009a; *Bologna et al*., 2011]. Note that, the calculated conductivity derived from cube model [*Waff*, 1974] yields similar results from the sphere-type model (HS+) [*Hashin and Shtrikmann*, 1962]. (b) Activation enthalpy for electrical conductivity in carbon-bearing systems versus graphite volume fraction.

$$\sigma_{HS}^{+}=\sigma_m+\frac{(1-\phi)}{\frac{1}{\sigma_s-\sigma_m}+\frac{\phi}{3\sigma_m}} \quad (5a)$$

The Hashin-Shtrikman lower bound (HS−), the opposite case of the HS upper bound, represents isolated spheres of conductive phase in a resistive matrix representing the grains, and takes the form

$$\sigma_{HS}^{-}=\sigma_s+\frac{\phi}{\frac{1}{\sigma_m-\sigma_s}+\frac{1-\phi}{3\sigma_s}} \quad (5b)$$

In this study, we calculate the bulk effective conductivity of two-phase (olivine + graphite) system at 1400 K from equations (2) to (5). The graphite conductivity is fixed at $10^{5.1}$ S/m [*Yoshino and Noritake*, 2011]. The olivine conductivity is fixed at $10^{-2.56}$ S/m from this study. Figure 10a illustrates the measured bulk conductivity versus graphite fraction together with various mixing models for the olivine + graphite system. According to the theoretical calculations (Figure 10a), only 2×10^{-4} to 7×10^{-4} vol % of carbon fraction in the tube model is needed to explain the high conductivity of 10^{-1} to $10^{-0.5}$ S/m observed in the high-conductive regions of the upper mantle [*Shankland and Waff*, 1977; *Jones et al*., 2003; *Evans et al*., 2005]. In the case of the Hashin-Shtrikman (HS) upper bound or parallel model, the graphite fraction is less than 4×10^{-4} vol %. This prediction is consistent with the calculation by *Duba and Shankland* [1982]. By contrast, the volume fraction of graphite required to explain the high-conductive regions of the upper mantle from laboratory measurement is considerably higher than that inferred from the HS upper bound or tube model by assuming the interconnection of conductive phase. The bulk conductivity observed in this study is close to that predicted from the HS lower bound or a series circuit when the volume fraction of graphite is low (less than 0.8 vol %). It is also consistent with the previous observations [*Watson et al*., 2010]. The increasing graphite volume fraction results in the increase in electrical conductivity of graphite-bearing samples (Figure 10a) and in the decrease in corresponding activation enthalpy (Figure 10b).

Wang et al. [2013] reported an abnormal behavior showing relatively low conductivity for olivine containing 4 vol % graphite, which is close to that estimated from the HS lower bound (Figure 10a). However, this sample has a fairly low activation enthalpy (~0.16 eV). This phenomenon can be caused by the temporal interconnection of graphite immediately after diamond-to-graphite transformation as a result of volume expansion.

The disconnection of the graphite film observed in the carbon-coated system demonstrates that the interconnectivity of graphite is controlled by the interfacial energy minimization in the system. *Dutta* [1953] reported that single-crystal graphite has high and anisotropic electrical conductivity, the conductivity along the basal plane $\sigma_{\perp}$ (i.e., perpendicular to the hexagonal axis) is four orders of magnitude higher than that perpendicular to the basal plane $\sigma_{\parallel}$ (i.e., parallel to the hexagonal axis). For example, at 560°C, log $\sigma_{\perp} \approx$ 5.9 S/m (0.7 log units higher than that (log$\sigma \approx$ 5.17 S/m) for polycrystalline graphite from *Yoshino and Noritake* [2011]) and log $\sigma_{\parallel} \approx$ 2.11 S/m. Specifically, it is found that both the conductivity parallel to the basal plane ($\sigma_{\perp}$) and the conductivity anisotropy ($\sigma_{\perp}/\sigma_{\parallel}$) in single crystals of graphite decreases largely with increasing temperature [*Dutta*, 1953]. Thus, it is reasonably expected that the conductivity parallel to the basal plane ($\sigma_{\perp}$) would be close to that of polycrystalline graphite and the conductivity anisotropy becomes smaller at high temperature. As a result, the connectivity of graphite is much important for the bulk conductivity than the anisotropic conductivity in this case. The electrical conductivity of polycrystalline graphite with no lattice preferred orientation is almost the same as that of crystallographic direction with high conductivity. The abnormally high sample conductivity at the onset of annealing also indicates that the graphite aligned to the conductive crystallographic direction (along the basal plane) parallel to the grain boundary. In addition, realignment of (0001) plane perpendicular to the olivine crystal surface during annealing seems to be difficult because dominant slip plane is (0001). The value of interfacial energy between graphite (0001) plane and olivine crystal surface has not been experimentally determined. On the other hand, the grain boundary film is only stable when the dihedral angle is zero. The huge dihedral angle more than 60° obtained from graphite-bearing system does not theoretically allow interconnection of graphite as a conductive phase. When dihedral angle is around 100°, the percolation threshold for pinch-off boundary exceeds more than 5 vol % [*von Bargen and Waff*, 1986] as shown in Figure 4b. Our conductivity measurement of polycrystalline olivine mixed with 0.8 vol % graphite shows a strong temperature dependence and relatively low conductivity. Therefore, the connectivity of graphite on olivine grain boundaries is readily destructed as a result of the higher interfacial energy between graphite and silicate minerals.

4.3. Geophysical *I*mplications

Hirschmann and Dasgupta [2009] estimated the carbon concentration for the depleted and enriched mantle through H/C ratio. They argued that the H/C ratio of the MORB source mantle is 0.75 $\pm$ 0.25, whereas that of the OIB source mantle is 0.5 $\pm$ 0.3. Therefore, they acquired the carbon concentration of 16 $\pm$ 9 ppm for the depleted mantle and 33–500 ppm for the enriched mantle. Although different researchers obtained different values, the average carbon content for the lithosphere mantle is less than 60 ppm [*Deines*, 2002; *Hazen et al*., 2012], which is considerably less than 0.8 vol % carbon. If all carbon exists as graphite, such a small amount (0.0005–0.08 vol %) also means that continuous interconnection is particularly important in producing high conductivity observed in some areas of the mantle. In other words, graphite must form interconnected films or layers over the distances of at least the resolution of MT or GDS experiments (tens or hundreds of kilometers), and these films or layers must be stably interconnected over such long distances on geological time scales.

Jones et al. [2003] reported a high-conductivity zone (10^{-1} S/m) at the depth of approximately 80–120 km in the upper part of the subcontinental lithospheric mantle in the central Slave craton (northern Canada), termed the Central Slave Mantle Conductor (CSMC), through the MT technique. This high-conductivity anomaly in the CSMC is interpreted through the presence of the interconnected graphite on the grain boundaries rather than the water or partial melt because the old tectonic-stable area is depleted with water. The temperature is also low (<1300 K) in the relatively shallow (~100 km) part of the upper mantle. In contrast to the case of Slave craton, the lithospheric conductive structure obtained by *Jones et al*. [2009a] showed the evidence of obvious spatial relationships between diamondiferous kimberlites fields and the lateral changes in either conductivity or conductivity anisotropy for the Kaapvaal Craton below southern Africa. These correlations imply that the electrical conductivity of the Kaapvaal craton is controlled not by minor constituents (i.e., graphite or water), as is often the case, but by the primary rock matrix. As discussed by *Jones et al*. [2009b], the Kaapvaal Craton exhibits far more uniform properties without strong chemical layering. It also has higher heat flow across the Moho than the other Archean cratons [*Jaupart and Mareschal*, 1999]. Therefore, the electrical conductivity of the lithospheric mantle of the Kaapvaal Craton is controlled by temperature.

Recently, *Bologna et al*. [2011] revealed several nearly horizontal high-conductivity anomalies in São Francisco craton in Brazil, which may be related to tectonic events. Most authors [e.g., *Jones et al*., 2003; *Chen et al*., 2009; *Bologna et al*., 2011] explained the enhanced conductivity in the lithospheric mantle in terms of the interconnected graphite on grain boundaries. Nonetheless, whether the interconnected graphite films can be stably maintained over such long geological time is questionable. The present experimental results and previous studies [*Watson et al*., 2010; *Yoshino and Noritake*, 2011] demonstrated that the graphite film on the grain boundary of minerals is unstable under lithospheric mantle conditions. Thus, the conductivity anomalies observed in the tectonically stable lithosphere cannot be interpreted with graphite hypothesis. Alternatively, as suggested by *Pinto et al*. [2010], the presence of a small amount of carbonatite melts (∼0.005 vol %) was mentioned in the conductive cratonic lithosphere-generating rejuvenation and reoxidation in the reduced mantle. Recent high-pressure experiments revealed a significant increase in conductivity by a small amount of carbonate melt [*Gaillard et al*., 2008; *Yoshino et al*., 2010, 2012; *Sifré et al*., 2014, 2015].

On the other hand, previous studies have already shown a reasonable overlap of the high-conductive regions and low-velocity zone (LVZ) in the upper mantle [*Oldenburg*, 1981; *Shankland et al*., 1981]. If the graphite model is applied to such a given case, a great difficulty may be encountered in explaining LVZ. The direct effect of graphite on other physical properties is generally insignificant because the amounts of graphite required for the observed high-conductive regions are very small. In particular, carbon has a small effect on lowering seismic velocities and increasing attenuation, whereas both may be easily produced through partial melt [*Takei*, 2002]. Therefore, the interpretation of high-conductive regions in the upper mantle may be locally different from one case to another, which depends on geological and petrological settings, tectonic framework, and evolutionary processes. If graphite is invoked to explain the observations of high-conductivity anomalies in the upper mantle, the physical and chemical causes for graphite transportation, precipitation, and interconnection over great distances should be carefully considered in view of pressure, temperature, and stress conditions.

5. Conclusion

In this study, we performed the conductivity measurements simultaneously on polycrystalline olivine mixed with graphite and carbon-coated olivine bicrystal at 1 and 3 GPa and up to 1700 K. The effect of graphite on the bulk electrical conductivity of a carbon-bearing sample is found to be negligible when the carbon content is less than 0.8 vol %. A strong temperature dependence (large activation enthalpy ∼ 1.32 eV) of conductivity suggests that graphite is disconnected on the olivine grain boundary. On the other hand, the electrical conductivity of carbon-coated olivine bicrystal is initially high and shows a weak temperature dependence, indicating the connectivity of graphite film on grain boundary. While during annealing at high temperature, the electrical conductivity displays a systematical change with the rate of decrease in conductivity, which varies as a function of the graphite thickness. For most runs, strong temperature dependence (large activation enthalpy) is similar to that of a single-crystal olivine. Both optical microscopic observations of recovered samples and the evolution of impedance arc demonstrated that the graphite film on olivine grain boundary is not stable at high temperature due to higher interfacial energy between graphite and olivine. Small activation enthalpy for the apparent disconnection rate of a graphite film on olivine grain boundaries suggests that the connectivity of graphite film is probably controlled via carbon grain boundary diffusion in silicates. Therefore, the present study indicates that graphite cannot account for the geophysically observed high-conductivity anomalies in the lithospheric mantle.

Acknowledgments

As per AGU's Data Policy, the corresponding author (Baohua ZHANG, Email: zhangbaohua@vip.gyig.ac.cn) may be contacted in order to access any relevant data related to this article. We thank W. Du Frane for his constructive comments. The authors are indebted to E. Ito, D. Yamazaki, A. Yoneda, X. Guo for benefit discussions. This study was supported by a grant-in-aids for Scientific Research grant 24244087 to TY from the Japan Society for Promotion of Science, and partially supported by the Strategic Priority Research Program (B) of the Chinese Academy of Sciences (XDB 18010401), the 1000Plan Program for Young Talents, Hundred Talent Program of CAS and NSF of China (41303048) to BZ. The authors declare that they have no competing interests.

References

Baba, K., A. D. Chave, R. L. Evans, G. Hirth, and R. L. Mackie (2006), Mantle dynamics beneath the East Pacific Rise at 17°S: Insights from the Mantle Electromagnetic and Tomography (MELT) experiment, *J. Geophys. Res.*, *111*, B02101, doi:10.1029/2004JB003598.

Barsoukov, E., and J. R. Macdonald (2005), *Impedance Spectroscopy: Theory, Experiment, and Applications*, pp. 1–583, John Wiley, New Jersey.

Bologna, M. S., A. L. Padilha, Í. Vitorello, and M. B. Pádua (2011), Signatures of continental collisions and magmatic activity in central Brazil as indicated by a magnetotelluric profile across distinct tectonic provinces, *Precambrian Res.*, *185*, 55–64.

Chantel, J., G. Manthilake, D. Andrault, D. Novella, T. Yu, and Y. Wang (2016), Experimental evidence supports mantle partial melting in the asthenosphere, *Sci. Adv.*, *2*, e1600246, doi:10.1126/sciadv.1600246.

Chen, C. W., S. Rondenay, R. L. Evans, and D. B. Snyder (2009), Geophysical detection of relict metasomatism from an Archean (∼3.5 Ga) subduction zone, *Science*, *326*, 1089–1091.

Constable, S. (2006), SEO3: A new model of electrical conductivity, *Geophys. J. Int.*, *166*, 435–437.

Dai, L. D., and S. Karato (2014), High and highly anisotropic electrical conductivity of the asthenosphere due to hydrogen diffusion in olivine, *Earth Planet. Sci. Lett.*, *408*, 79–86.
Dai, L. D., H. P. Li, H. Y. Hu, and S. M. Shan (2010), The electrical conductivity of dry polycrystalline olivine compacts at high temperatures and pressures, *Mineral. Mag.*, *74*, 849–857.
Day, H. W. (2012), A revised diamond-graphite transition curve, *Am. Mineral.*, *97*, 52–62.
Deines, P. (2002), The carbon isotope geochemistry of mantle xenoliths, *Earth Sci. Rev.*, *58*, 247–278.
Drury, M. J. (1978), Partial melt in the asthenosphere: Evidence from electrical conductivity data, *Phys. Earth Planet. Inter.*, *17*, 16–20.
Du Frane, W. L., J. J. Roberts, D. A. Toffelmier, and J. A. Tyburczy (2005), Anisotropy of electrical conductivity in dry olivine, *Geophys. Res. Lett.*, *32*, L24315, doi:10.1029/2005GL023879.
Duba, A., and T. J. Shankland (1982), Free carbon and electrical conductivity in the Earth's mantle, *Geophys. Res. Lett.*, *9*, 1271–1274.
Ducea, M. N., and S. K. Park (2000), Enhanced mantle conductivity from sulfide minerals, southern Sierra Nevada, California, *Geophys. Res. Lett.*, *27*, 2405–2408, doi:10.1029/2000GL011565.
Dutta, A. K. (1953), Electrical conductivity of single crystals of graphite, *Phys. Rev.*, *90*, 187–192.
Evans, R. L., G. Hirth, K. Baba, D. Forsyth, A. Chave, and R. Mackie (2005), Geophysical evidence from the MELT area for compositional controls on oceanic plates, *Nature*, *437*, 249–252.
Frost, B. R., W. S. Fyfe, K. Tazaki, and T. Chan (1989), Grain-boundary graphite in rocks and implications for high electrical conductivity in the lower crust, *Nature*, *340*, 134–136.
Frost, D. J., and B. J. Wood (1997), Experimental measurements of the fugacity of CO_2 and graphite/diamond stability from 35 to 77 kbar at 925 to 1650°C, *Geochim. Cosmochim. Acta*, *61*, 1565–1574.
Frost, D. J., and C. McCammon (2008), The redox state of Earth's mantle, *Annu. Rev. Earth Planet. Sci.*, *36*, 389–420.
Gaillard, F., M. Marki, G. Iacono-Marziano, M. Pichavant, and B. Scaillet (2008), Carbonatite melts and electrical conductivity in the asthenosphere, *Science*, *322*, 1363–1365.
Gardés, E., F. Gaillard, and P. Tarits (2014), Toward a unified hydrous olivine electrical conductivity law, *Geochem. Geophys. Geosyst.*, *15*, 4984–5000, doi:10.1002/2014GC005496.
Glover, P. W. J. (1996), Graphite and electrical conductivity in the lower continental crust: A review, *Phys. Chem. Earth*, *21*, 279–287.
Hashin, Z., and S. Shtrikman (1962), A variational approach to the theory of effective magnetic permeability of multiphase materials, *J. Appl. Phys.*, *33*, 3125–3131, doi:10.1063/1.1728579.
Hayden, L. A., and E. B. Watson (2008), Grain boundary mobility of carbon in Earth's mantle: A possible carbon flux from the core, *Proc. Natl. Acad. Sci. U. S. A.*, *105*, 8537–8541.
Hazen, R. M., R. J. Hemley, and A. J. Mangum (2012), Carbon in Earth's interior: Storage, cycling, and life, *EOS Trans. AGU*, *93*, 17–18.
Hirschmann, M. M., and R. Dasgupta (2009), The H/C ratios of Earth's near-surface and deep reservoirs, and consequences for deep Earth volatile cycles, *Chem. Geol.*, *262*, 4–16.
Jaupart, C., and J. C. Mareschal (1999), The thermal structure and thickness of continental roots, *Lithos*, *48*, 93–114.
Jones, A. G. (1999), Imaging the continental upper mantle using electromagnetic methods, *Lithos*, *48*, 57–80, doi:10.1016/s0024-4937(99)00022-5.
Jones, A. G., and I. J. Ferguson (2001), The electric Moho, *Nature*, *409*, 331–333.
Jones, A. G., P. Lezaeta, I. J. Ferguson, A. J. Chave, R. L. Evans, X. Garcia, and J. Spratt (2003), The electrical structure of the Slave craton, *Lithos*, *71*, 505–527.
Jones, A. G., et al. (2009a), Area selection for diamonds using magnetotellurics: Examples from southern Africa, *Lithos*, *112S*, 83–92.
Jones, A. G., R. L. Evans, and D. W. Eaton (2009b), Velocity-conductivity relationships for mantle mineral assemblages in Archean cratonic lithosphere based on a review of laboratory data and application of extremal bound theory, *Lithos*, *109*, 131–143.
Jurewicz, S. R., and A. J. G. Jurewicz (1986), Distribution of apparent angles on random sections with emphasis on dihedral angle measurements, *J. Geophys. Res.*, *91*, 9277–9282.
Kanter, M. A. (1957), Diffusion of carbon atoms in natural graphite crystals, *Phys. Rev.*, *107*, 655–663.
Karato, S. (1990), The role of hydrogen in the electrical conductivity of the upper mantle, *Nature*, *347*, 272–273.
Karato, S., and D. Wang (2013), Electrical conductivity of minerals and rocks, in *Physics and Chemistry of the Deep Earth*, edited by S. Karato, pp. 145–182, Wiley-Blackwell, New York.
Kawano, S., T. Yoshino, and I. Katayama (2012), Electrical conductivity of magnetite-bearing serpentinite during shear deformation, *Geophys. Res. Lett.*, *39*, L20313, doi:10.1029/2012GL053652.
Naif, S., K. Key, S. Constable, and R. L. Evans (2013) Melt-rich channel observed at the lithosphere-asthenosphere boundary, *Nature*, *495*, 356–359.
Ni, H. W., H. Keppler, and H. Behrens (2011), Electrical conductivity of hydrous basaltic melt: Implications for partial melting in the upper mantle, *Contrib. Mineral. Petrol.*, *162*, 637–650.
Oldenburg, D. W. (1981), Conductivity structure of oceanic upper mantle beneath the Pacific plate, *Geophys. J. R. Astron. Soc.*, *65*, 359–394.
Pearson, D. G., F. R. Boyd, S. E.Haggerty, J. D. Pasteris, S. W. Field, P. H. Nixon, and N. P. Pokhilenko (1994). The characterisation and origin of graphite in cratonic lithospheric mantle: A petrological carbon isotope and Raman spectroscopic study. *Contrib. Mineral. Petrol.*, *115*, 449–466.
Pinto, L. G. R., M. B. Pádua, N. Ussami, I. Vitorello, A. L. Padilha, and C. Braitenberg (2010), Magnetotelluric deep soundings, gravity and geoid in the South São Francisco craton: Geophysical indicators of cratonic lithosphere rejuvenation and crustal underplating, *Earth Planet Sci. Lett.*, *297*, 423–434.
Poe, B. T., C. Romano, F. Nestola, and J. R. Smyth (2010), Electrical conductivity anisotropy of dry and hydrous olivine at 8 GPa, *Phys. Earth Planet. Inter.*, *181*, 103–111, doi:10.1016/j.pepi.2010.05.003.
Pommier, A., F. Gaillard, M. Malki, and M. Pichavant (2010), Reevaluation of the electrical conductivity of silicate melts, *Am. Mineral.*, *95*, 284–291.
Roberts, J. J., A. G. Duba, E. A. Mathez, T. J. Shankland, and R. Kinsler (1999), Carbon-enhanced electrical conductivity during fracture of rocks, *J. Geophys. Res.*, *104*, 737–747.
Schmeling, H. (1986), Numerical models on the influence of partial melt on elastic, anelastic and electric properties of rocks. Part II: Electrical conductivity, *Phys. Earth Planet. Inter.*, *43*, 123–136.
Schock, R. N., A. G. Duba, and T. J. Shankland (1989), Electrical conduction in olivine, *J. Geophys. Res.*, *94*, 5829–5839.
Schulgasser, K. (1976), Relationship between single-crystal and polycrystal electrical conductivity, *J. Appl. Phys.*, *47*, 1880–1886.
Schulgasser, K. (1977), Bounds on the conductivity of statistically isotropic polycrystals, *J. Phys. C*, *10*, 407–417.

Shankland, T. J., and H. S. Waff (1977), Partial melting and electrical conductivity anomalies in the upper mantle, *J. Geophys. Res.*, *82*, 5409–5417.
Shankland, T. J., and M. E. Ander (1983), Electrical conductivity, temperatures, and fluids in the lower crust, *J. Geophys. Res.*, *88*, 9475–9484.
Shankland, T. J., R. J. O'Connell, and H. S. Waff (1981), Geophysical constraints on partial melt in the upper mantle, *Rev. Geophys. Space Phys.*, *19*, 394–406.
Shimojuku, A., T. Yoshino, D. Yamazaki, and T. Okudaira (2012), Electrical conductivity of fluid-bearing quartzite under lower crustal conditions, *Phys. Earth Planet. Inter.*, *198–199*, 1–8.
Shimojuku, A., T. Yoshino, and D. Yamazaki (2014), Electrical conductivity of brine-bearing quartzite at 1 GPa: Implications for fluid content and salinity of the crust, *Earth Planets Space*, *66*, 2–9.
Selway, K. (2014), On the causes of electrical conductivity anomalies in tectonically stable lithosphere, *Surv. Geophys.*, *35*, 219–257.
Sifré, D., E. Gardes, M. Massuyeau, L. Hashim, S. Hier-Majumder, and F. Gaillard (2014), Electrical conductivity during incipient melting in the oceanic low-velocity zone, *Nature*, *509*, 81–85.
Sifré, D., L. Hashim, and F. Gaillard (2015), Effects of temperature, pressure and chemical compositions on the electrical conductivity of carbonated melts, *Chem. Geol.*, *418*, 189–197, doi:10.1016/j.chemgeo.2014.09.022.
Takei, Y. (2002), Effect of pore geometry on Vp/Vs: From equilibrium geometry to crack, *J. Geophys. Res.*, *107*(B2), 2043, doi:10.1029/2001JB000522.
Von Bargen, N., and H. S. Waff (1986), Permeabilities, interfacial areas and curvatures of partially molten systems: Results of numerical computations of equilibrium microstructures, *J. Geophys. Res.*, *91*, 9261–9276.
Waff, H. S. (1974), Theoretical considerations of electrical conductivity in a partially molten mantle and implications for geothermometry, *J. Geophys. Res.*, *79*, 4003–4010.
Wang, D., M. Mookherjee, Y. Xu, and S. Karato (2006), The effect of water on the electrical conductivity of olivine, *Nature*, *443*, 977–980.
Wang, D., S. Karato, and Z. Jiang (2013), An experimental study of the influence of graphite on the electrical conductivity of olivine aggregates, *Geophys. Res. Lett.*, *40*, 2028–2032, doi:10.1002/grl.50471.
Watson, E. B., and J. M. Brennan (1987), Fluids in the Lithosphere. 1: Experimentally determined wetting characteristics of CO_2-H_2O fluids and their implications for fluid transport, host rock physical properties, and fluid inclusion formation, *Earth Planet Sci. Lett.*, *85*, 497–515.
Watson, H. C., J. J. Roberts, and J. A. Tyburczy (2010), Effect of conductivity impurities on electrical conductivity in polycrystalline olivine, *Geophys. Res. Lett.*, *37*, L02302, doi:10.1029/2009GL041566.
Xu, Y., T. J. Shankland, and A. G. Duba (2000), Pressure effect on electrical conductivity of mantle olivine, *Phys. Earth Planet. Inter.*, *118*, 149–161.
Yoshino, T. (2010), Laboratory electrical conductivity measurement of mantle minerals. *Surv. Geophys.*, *31*, 163–206.
Yoshino, T., and F. Noritake (2011), Unstable graphite films on grain boundaries in crustal rocks, *Earth Planet. Sci. Lett.*, *306*, 186–192.
Yoshino, T., M. J. Walter, and T. Katsura (2003), Core formation in planetesimals triggered by permeable flow, *Nature*, *422*, 154–157.
Yoshino, T., M. J. Walter, and T. Katsura (2004), Connectivity of molten Fe alloy in peridotite based on in situ electrical conductivity measurements: Implications for core formation in terrestrial planets, *Earth Planet. Sci. Lett.*, *222*, 625–643.
Yoshino, T., T. Matsuzaki, S. Yamashita, and T. Katsura (2006), Hydrous olivine unable to account for conductivity anomaly at the top of the asthenosphere, *Nature*, *443*, 973–976, doi:10.1038/nature05223.
Yoshino, T., T. Matsuzaki, A. Shatskiy, and T. Katsura (2009), The effect of water on the electrical conductivity of olivine aggregates and its implications for the electrical structure of the upper mantle, *Earth Planet. Sci. Lett.*, *288*, 291–300.
Yoshino, T., M. Laumonier, E. McIsaac, and T. Katsura (2010), Electrical conductivity of basaltic and carbonatite melt-bearing peridotites at high pressures: Implications for melt distribution and melt fraction in the upper mantle, *Earth Planet. Sci. Lett.*, *295*, 593–602, doi:10.1016/j.epsl.2010.04.050.
Yoshino, T., E. McIsaac, M. Laumonier, and T. Katsura (2012), Electrical conductivity of partial molten carbonatite peridotite, *Phys. Earth Planet. Inter.*, *194–195*, 1–9.
Zhang, B. H., T. Yoshino, D. Yamazaki, G. Manthilake, and T. Katsura (2014), Electrical conductivity anisotropy in partially molten peridotite under shear deformation, *Earth Planet. Sci. Lett.*, *405*, 98–109.
Zhao, Y. X., and I. L. Spain (1989), X-ray diffraction data for graphite to 20 GPa, *Phys. Rev. B*, *40*, 993–997.